JACS
JOURNAL OF THE AMERICAN CHEMICAL SOCIETY
pubs.acs.org/JACS
Article

Open Access
This article is licensed under CC-BY 4.0

Ambipolar Electrochemical Doping of $CsPbBr_3$ Nanocrystals

Yan B. Vogel,* Yesim Sahin, Oleksandra Ortikova, Simon C. Boehme, Arjan J. Houtepen, Dmitry N. Dirin, and Maksym V. Kovalenko*

Cite This: J. Am. Chem. Soc. 2026, 148, 49828−49838

Read Online

ACCESS | Metrics & More | Article Recommendations | Supporting Information

ABSTRACT: Electronic doping underpins many semiconductor applications but has remained elusive for lead halide perovskite nanocrystals because their high density and low formation energy of defects easily compensate introduced dopants. Here, we use electrochemical doping as a strategy to avoid doping compensation. Electrochemical injection of electrons or holes into the nanocrystal is compensated by surface-adsorbed electrolyte counterions, therefore not compromising crystal structure. We accomplished ambipolar (n- and p-type) doped $CsPbBr_3$ nanocrystals with charge carrier concentrations ranging from intrinsic up to 4.8×10^{17} cm^{-3} (corresponding to 0.25 charges per nanocrystal). We show that electrochemical doping is reversible and stable at these free carrier concentrations. The extent of doping and stability are enabled by the use of lecithin, a zwitterionic ligand that strongly binds to the surface of the $CsPbBr_3$ nanocrystals while still allowing ion and electron transfer. Lecithin stabilizes the surface atoms by shifting the potentials for Pb^{2+} reduction and Br^- oxidation outside of the bandgap. The inferred surface-chemistry design rules for stable electrochemical doping can also serve as a guideline for developing $CsPbBr_3$ nanocrystals stable under high free-carrier concentrations in optoelectronic devices, such as light-emitting diodes or electronically triggered quantum light sources.

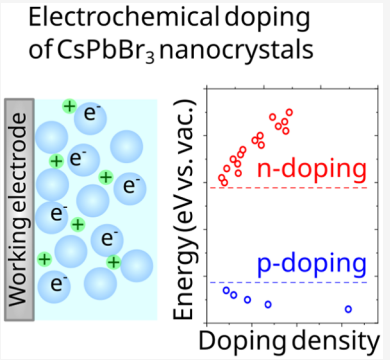

INTRODUCTION

Cesium lead halide perovskite nanocrystals (NCs), with the general formula $CsPbX_3$ (X = Cl, Br, I), show an exceptional combination of optoelectronic properties, including strong absorption,[1,2] narrowband photoluminescence,[3−5] near-unity photoluminescence quantum yield,[6−9] and emission wavelength tunable by composition.[10,11] In addition, their low formation energy enables facile low-cost synthesis and scalable manufacturing.[12−14] As such, $CsPbX_3$ NCs are promising materials for optoelectronic devices.[10,11,15]

Control of the free-carrier density, both in terms of the electronic doping type (p and n) and its magnitude, is a crucial degree of freedom in optoelectronic device engineering. However, electronic doping of $CsPbX_3$ NCs remains a significant challenge.[16,17] Some works have demonstrated electronic doping by substituting Pb^{2+} ions with Ag^+ or Bi^{3+} ions.[18−20] However, substitutional doping is detrimental to the NC's optical and structural properties. The large number of intrinsic defects and their low formation energy in $CsPbX_3$ easily compensate substitutional dopants.[21] Moreover, the low lattice energy facilitates expulsion of such dopants.[22] Another strategy to control the free-carrier density is through molecular doping, the use of redox molecules to transfer charge to $CsPbX_3$ NCs.[23−26] However, the addition of electron donors or acceptors to a nanocrystal system introduces unwanted charge-transfer pathways, might increase trap density, and can substantially change the electronic structure of the nanocrystal.

Electrochemical doping offers a high degree of control over doping in semiconductor NCs.[27−30] The applied potential sets the Fermi level[31] and allows modulation of the electronic doping from intrinsic carrier density to complete band filling.[28] Electrochemical doping can be either reversible or permanent.[32,33] In addition, electrochemical doping does not compromise the structure of the NCs because the injection of electrons or holes into the NCs is compensated by surface-adsorbed electrolyte counterions which ensure overall charge neutrality. Indeed, several works have demonstrated electrochemical doping of a variety of NCs, including ZnO,[31,34,35] CdSe,[30] Si,[36] Pb(S, Se),[27,37,38] CdTe,[39,40] Hg(S, Se, Te),[41,42] $CsPbBr_3$,[43] and InAs.[28,44]

Electrochemical doping, however, can result in electrochemical degradation if the applied potential is not within the stable electrochemical window.[27,28,38,45,46] Electrochemical doping of $CsPbX_3$ NCs remains poorly controlled and limited by the anodic and cathodic degradation reactions prevalent in $CsPbX_3$ NCs. Mulder et al. demonstrated electrochemical p-doping of $CsPbBr_3$ NCs at charge carrier concentrations up to 0.2 holes/NC.[43] However, p-doping was metastable, and it

Received: September 13, 2026
Revised: October 30, 2026
Accepted: November 2, 2026
Published: November 8, 2026

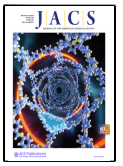

ACS Publications
© 2026 The Authors. Published by American Chemical Society

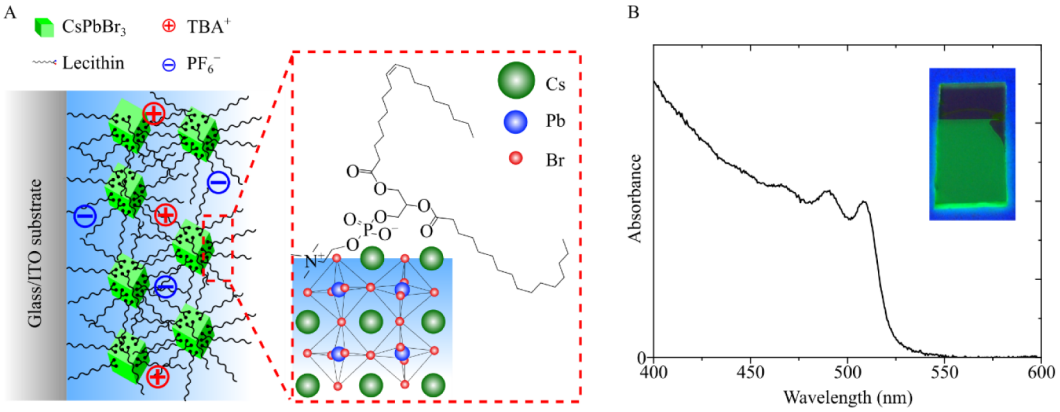

Figure 1. Experimental model. (A) Schematic representation of the $CsPbBr_3$-lecithin NCs film used in this study to explore electrochemical doping. The $CsPbBr_3$-lecithin NC films are deposited on an ITO/glass substrate and immersed in an electrolyte containing 0.1 M $TBAPF_6$ in propylene carbonate, unless otherwise specified. Reproduced from ref. 67. Copyright 2024 American Chemical Society. (B) Absorption spectrum and photograph under ultraviolet illumination (inset) of the $CsPbBr_3$-lecithin NCs film on the ITO/glass substrate.

remained unclear under what conditions it could be stabilized. Successful p-doping depended on the specific NC synthesis and ligand exchange. Hettiger et al. and Jayabalan et al. showed reversible photoluminescence (PL) quenching under anodic bias, which could be due to p-doping.[47−49] However, reversible PL quenching is not unambiguous evidence of doping.[46] In addition, previous attempts at electrochemical n-doping led to the reduction of Pb^{2+}.[43,50] The work of Heo et al. stands out as they report ambipolar doping, yet the potentials span less than the bandgap value.[51]

In $CsPbBr_3$ NCs, the anodic and cathodic degradation reactions are the oxidation of Br^- ($CsPbBr_3 \rightleftharpoons Pb^{2+} + Cs^+ + 3/2Br_2 + 3e^-$) and the reduction of Pb^{2+} ($CsPbBr_3 + 2e^- \rightleftharpoons Pb + Cs^+ + 3Br^-$), respectively.[45,50] These reactions result in the electrochemical degradation of the $CsPbBr_3$ NCs, preventing stable electrochemical doping. From a thermodynamic perspective, electrochemical degradation upon charge injection is minimized when the standard potentials of these reactions lie well outside the bandgap.

The standard potentials of redox species and the $1S_e$ and $1S_h$ levels of NCs are both highly tunable, which opens the possibility of stabilizing electrochemical doping. We note that throughout the text, we refer to the lowest-energy electron state as $1S_e$, to the lowest-energy hole level as $1S_h$, and to the lowest-energy optical transition (probed in absorption) as $1S_h1S_e$ or, in short, 1S. Previous research showed that the position of the $1S_e$ and $1S_h$ levels of NCs can be tuned by using different surface ligands,[52,53] immersing the NCs in different solvents[27] and electrolytes,[54] or introducing alkali ions.[55] Moreover, binding a ligand to the NC surface would shift the equilibrium of the degradation reactions to the left side, lowering the free energy and therefore making the standard potential more negative for reduction and more positive for oxidation. Degbevi et al. recently showed an elegant example of the decrease in standard potential of CdSe NCs with increasing coordination energy of carbonyl complexes that act as X-type ligands.[56] A similar strategy has been widely applied to stabilize bulk single-crystal silicon surfaces by using ligands that make a strong Si−C bond,[57,58] allowing the widespread use of silicon wafers as electrodes in electrochemistry.[59−61] We posited that enhancing the electrochemical stability could then allow ambipolar electrochemical doping of $CsPbBr_3$ NCs, presently a significant and unmet challenge.

Zwitterionic ligands,[62] particularly phospholipids,[63] are known to enhance the stability of $CsPbBr_3$ NCs. A recent study systematically surveyed ligands commonly used for $CsPbBr_3$ NCs using DOSY NMR, classifying them by independently probing their binding strength and dynamicity.[64] It was found that ligands featuring phosphoethanolamine and phosphocholine groups excel in both strength and staticity of binding, whereas those with sulfobetaine and guanidinium head groups bind relatively strongly yet dynamically. We therefore envisioned phosphoethanolamine and phosphocholine as particularly promising ligands for spectroelectrochemistry. For comparison, we also include the oleylammonium/oleate ligand pair and the sulfobetaine ligand used in the previous study.

We find that phosphoethanolamine and phosphocholine ligands stabilize $CsPbBr_3$ NCs against both electrolyte dissolution and electrochemical degradation. Conversely, films of $CsPbBr_3$ NCs passivated with the oleylammonium/oleate ligand pair and the sulfobetaine ligands readily dissolved in the electrolytes tested. $CsPbBr_3$ NCs passivated with lecithin ligands can be electrochemically doped with up to 0.15 electrons per NC and up to 0.25 holes per NC. However, we find that doping is limited to the NCs in direct contact with the electrode because the bulky lecithin ligands ($C_{42}H_{80}NO_8P$) impede charge transport across the film.

RESULTS AND DISCUSSION

Experimental Model

We synthesized $CsPbBr_3$ NCs capped with lecithin ligands, referred to as $CsPbBr_3$-lecithin NCs hereafter, adapting a previously reported procedure (see Section S1 in the SI for details).[65] The resulting $CsPbBr_3$-lecithin NCs are truncated cubes, nearly spherical, of 10 nm in diameter (Figure S1). Lecithin is a zwitterionic phosphocholine ligand with a $-PO_4^-$ group that binds to the surface Pb atom and a $-N(CH_3)_3^+$ group that substitutes the Cs atom of the $CsPbBr_3$ NC (Figure 1A).[66,67] The simultaneous binding of these two head groups results in one of the tightest ligand-binding regimes known for $CsPbBr_3$ NCs.[64] We expect the tight binding to stabilize the NC against anodic and cathodic degradation. We prepared $CsPbBr_3$-lecithin NC thin films by spin coating a dispersion of these NCs in toluene on an indium tin oxide (ITO) on glass substrate. The films are estimated to be 4.5 monolayers thick on average, unless otherwise specified, see Section S7 of the SI. Figure 1B (inset) shows a photograph of this film under ultraviolet illumination. Figure 1B

https://doi.org/10.1021/jacs.6c19292
J. Am. Chem. Soc. 2026, 148, 49828−49838

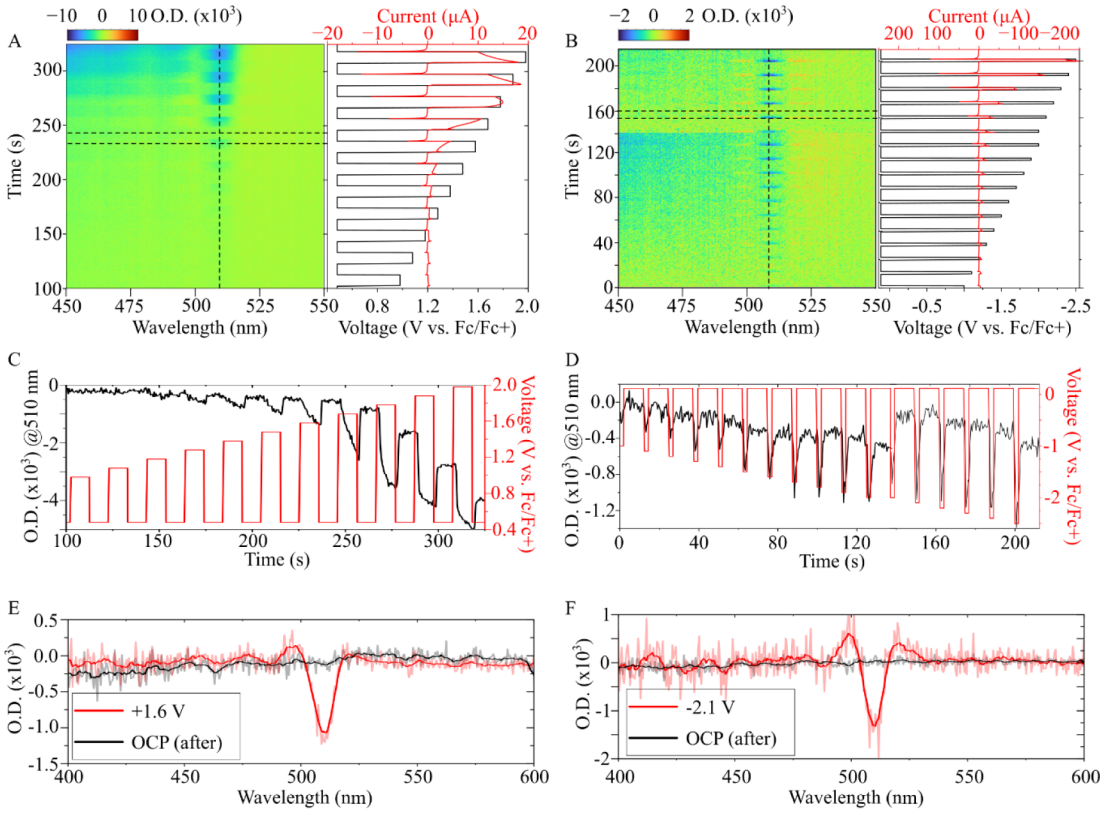

Figure 2. Electrochemical window and doping of $CsPbBr_3$-lecithin NC thin films. (A, B) 2D false-color plots of the differential absorbance spectra during the application of an (A) anodic and (B) cathodic potential modulation. The potential modulation is shown on the plot at the right side of the image (black line) and consists of potential steps of 10 s at OCP and (A) 10 s at an anodic potential or (B) 2 s at a cathodic potential. The anodic (cathodic) potential is initially 100 mV more positive (negative) than OCP, and increases (decreases) 100 mV per step. The red line shows the recorded current. The vertical and horizontal dashed lines on the 2D false-color plot indicate the traces shown in panels C–D and panels E–F, respectively. In B and D, the background was refreshed at 140 s (during OCP) by setting the absorbance change to zero. (C, D) Differential absorbance at the 1S transition (black line, averaged between 503 and 513 nm) during the potential steps (red line). (E, F) Differential absorbance spectra at (E) +1.6 V and (F) −2.1 V (red line), and at OCP after the application of such potentials (black line). The faint color is the raw data, and the darker color is the data smoothed over 10 adjacent wavelengths. The electrolyte is 0.1 M $TBAPF_6$ in propylene carbonate.

shows the visible absorption spectrum of $CsPbBr_3$-lecithin NC film. The lowest-energy absorption peak centered at 508 nm is the spectrally well-resolved 1S transition, followed by the next three transitions of 1P, 1D, and 1F character, respectively.[65,68]

We used the $CsPbBr_3$-lecithin NC thin film (inset in Figure 1B) as the working electrode in a custom-made, single-compartment, three-electrode, spectroelectrochemical cell. The spectroelectrochemical cell has two optical windows for measuring the transmittance of the $CsPbBr_3$-lecithin NC film in the visible range *in situ* during electrochemical modulation. The spectroelectrochemical cell and setup are described in detail elsewhere.[28]

Film Stability in Electrolyte

As a prerequisite for electrochemical doping of a $CsPbBr_3$ NC thin film, we tested its stability in the electrolyte for four different ligands and three different electrolyte solvents by following the changes in absorbance. The NC film instability could be due to both NC redispersion and ionic dissolution. Thus, the challenge was to find a ligand/solvent that neither redisperses the NCs nor strips their ligands. The ligands tested include the weaker binding oleic acid and oleylamine ligand couple ($CsPbBr_3$–OA/OLA) as well as the zwitterionic sulfobetaine ligand ($CsPbBr_3$-ASC18) and the stronger-binding zwitterionic ligands lecithin ($CsPbBr_3$-lecithin) and phosphoethanolamine ($CsPbBr_3$–PEA, Figure S2). We considered three commonly employed electrolyte solvents: propylene carbonate (PC), dichloromethane (DCM), and acetonitrile (MeCN). We chose $TBAPF_6$ (0.1 M) as the electrolyte salt because of its weakly coordinating nature.[45,69,70]

After insertion of a thin film in the electrolyte, we monitored its stability by continuously recording the absorption spectrum at open-circuit potential (OCP, see Section S3). $CsPbBr_3$ NCs passivated with OA/OLA and ASC18 readily dissolved in all solvents. In contrast, the $CsPbBr_3$-lecithin NC film exhibits much greater stability in both the $TBAPF_6$/PC and $TBAPF_6$/DCM electrolytes, with an absorbance decrease at 400 nm of less than 5% over 15 min. Only in $TBAPF_6$/MeCN did the film absorbance decrease significantly, by more than 60% over the same time frame. $CsPbBr_3$–PEA NC thin films remain stable in both $TBAPF_6$/PC and $TBAPF_6$/MeCN, but not in $TBAPF_6$/DCM. Table S2 in the SI summarizes these stability trends. These stability trends can be partially explained by the protecting role of the ligands preventing ionic dissolution; phosphocholine and phosphoethanolamine ligands are strongly and statically bound, while oleate/oleylamine and sulfobetaine binding is weaker and more dynamic.[64] We also cannot rule out that film redispersion plays a role. Yet, regardless of the instability mechanism, these measurements give the experimental conditions for electrochemical doping. In the following, we performed the electrochemical experiments only on the stable systems.

https://doi.org/10.1021/jacs.6c19292
J. Am. Chem. Soc. 2026, 148, 49828–49838

Electrochemical Stability of $CsPbBr_3$-lecithin NCs

Hole (electron) injection into the NC upon the application of a potential can lead to either doping or material degradation. For hole (electron) doping, the hole (electron) is delocalized in the $1S_h$ ($1S_e$) level, while for anodic (cathodic) degradation it is localized on the Br^- (Pb^{2+}) atom, resulting in its oxidation (reduction). Therefore, having shown that surface passivation with lecithin ligands prevents $CsPbBr_3$ NC thin film dissolution in $TBAPF_6$/PC, we next test the ligands' stabilizing effect against anodic and cathodic degradation.

We use *in situ* visible differential absorption spectroscopy to distinguish between electrochemical doping and degradation in $CsPbBr_3$ NCs. Upon the application of an anodic (cathodic) potential, electrochemical doping leads to a decrease in the absorbance of the 1S transition because of hole (electron) occupation of the quantum-confined $1S_h$ ($1S_e$) state. When the potential is reverted to the initial OCP, the absorbance returns to its initial value, making this change reversible. Electrochemical degradation of $CsPbBr_3$ NCs, however, leads to an irreversible decrease in the absorption spectrum, making *in situ* absorption spectroscopy an ideal tool for distinguishing between electrochemical doping and degradation.

We determined the stable electrochemical window of $CsPbBr_3$-lecithin NCs by applying potential steps from OCP to increasingly anodic or cathodic potentials and back to OCP while simultaneously recording the current and changes to the thin film's absorbance spectrum, see Figure 2A, C, E (anodic measurements) and Figure 2B, D, F (cathodic measurements). The plots on the right part of Figure 2A and 2B show the applied potential steps (black curve) and measured current (red curve) over time. The left part of Figure 2A and 2B shows a 2D color image of the change in the absorbance spectrum (color) during these potential steps.

The anodic (cathodic) currents (red plots in Figure 2A and 2B) indicate that, upon application of a potential, holes (electrons) are injected into the system. The total injected/extracted electrons in each step is the integrated current over time. Upon reverting to OCP, we observe a current of opposite sign but a charge of lower magnitude, indicating that holes (electrons) are partially extracted back. A cyclic voltammogram shows similar (quasi)reversible behavior (Figure S8). The (quasi)reversible electrochemical data indicate the hole (electron) transfer is followed by a chemical reaction, not allowing the hole (electron) to be extracted back upon reverting to OCP, and this is a general feature observed in NCs that we have previously discussed in detail.[38] However, currents alone do not carry information on the fate of those charges, for which we turn to look at the NC optical properties. Electrochemical degradation reactions would result in irreversible changes in the spectrum, while electrochemical doping is usually reversible.

We assess reversibility by examining the horizontal and vertical slices of the 2D color plots (dashed lines in Figure 2A and B). Vertical slices show the differential absorbance at the 1S transition during the potential steps (Figure 2C, D). Horizontal slices show the differential absorbance spectrum at an applied potential and after returning to OCP (Figure 2E, F). Figure 2C, D shows that the differential absorbance at the 1S transition decreases upon stepping the potential above +1.3 V or below −1.0 V vs ferrocene/ferrocenium (Fc/Fc^+, all potentials are referred to the Fc/Fc^+ redox couple), and recovers upon stepping back to OCP. Potentials between +1.0 V and −0.9 V do not show any spectral changes (Figures S9 and S10). Figure 2E and F shows that the differential absorbance spectrum returns to its original value after applying a potential of +1.6 V and −2.1 V, respectively. Figures S11-S16 show that the differential absorbance spectrum returns to above 90% of its original value for all potentials between +1.7 V and −2.5 V.

In situ photoluminescence spectroscopy during similar potential steps (Figure S17) also shows reversible changes, with the PL returning to 94−99% of its initial value after each step. The PL also shows an irreversible long-term quenching, resulting in a decrease to 91% (65%) of its initial value after the anodic (cathodic) experiment. The irreversible long-term quenching could be due to material loss from the film or slow ligand dissolution in the electrolyte, leading to surface traps. X-ray photoelectron spectroscopy (XPS) of these films after the anodic and cathodic potential steps does not show any changes in the oxidation state of Pb and Br (Figure S18).

Thus, the differential absorption and PL spectroelectrochemistry, and XPS results demonstrate that $CsPbBr_3$-lecithin NC films are stable in $TBAPF_6$/PC between +1.7 V and −2.5 V. In the following, we restrict our experiments to this stable electrochemical window.

Spectroelectrochemical Signatures and Extent of Electrochemical Doping

As the $1S_e$ ($1S_h$) level is filled with electrons (holes), the 1S transition is blocked, causing a decrease in absorbance and PL. The reversible decrease in absorbance and PL of the 1S transition upon both cathodic and anodic bias shown in Figure 2 and Figure S17 is, therefore, unambiguous evidence of electron and hole injection into the $1S_e$ and $1S_h$ levels, respectively. This demonstrates that $CsPbBr_3$-lecithin NCs can be electrochemically n- and p-doped. Now we turn our attention to quantifying the extent of doping and how it depends on the applied potential and time.

The 1S transition bleach remains relatively weak, reaching only 2% of the total 1S transition absorbance even when the anodic (or cathodic) potential is highest (lowest) (Figure 3A

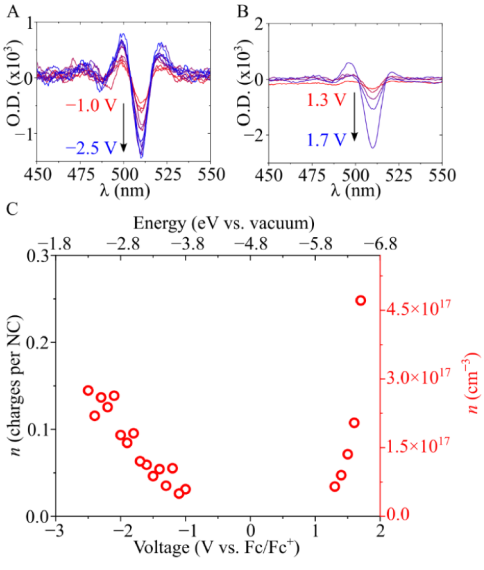

Figure 3. Charge carrier density in n- and p-doped $CsPbBr_3$-lecithin NCs. (A, B) Differential absorbance spectra as a function of the applied potential for (A) electron and (B) hole injection. (C) Charge carrier density as a function of the applied potential.

https://doi.org/10.1021/jacs.6c19292
J. Am. Chem. Soc. 2026, 148, 49828−49838

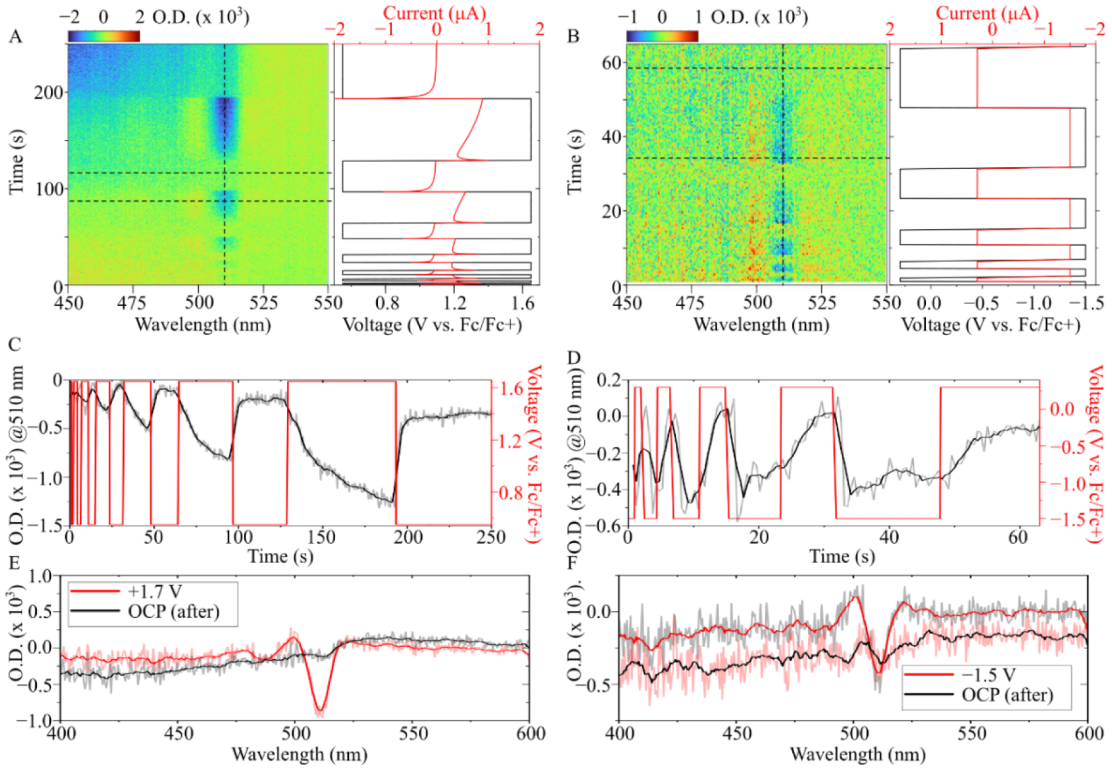

Figure 4. Time dependence of electrochemical doping. (A, B) 2D false-color plots of the differential absorbance spectra during (A) anodic and (B) cathodic potential modulation. The potential modulation is shown on the right (black line). The duration of the first step is 1 s and is doubled after each step. The red line is the measured current. The dashed lines on the 2D false-color plot indicate the traces shown in panels (C)-(F). (C, D) Differential absorbance at the 1S transition (black line) and applied potential (red line) as a function of time. The differential absorbance in (C) is reported both at 510 nm (faint line) and as an average between 505 and 510 nm (dark line). The differential absorbance in (D) is both reported as an average between 508 and 514 nm (faint line) and after additional temporal averaging across 5 time points (dark line). (E, F) Differential absorbance spectra at the 5th step (red lines) and at OCP after the step (black lines). The faint line is the raw data, and the dark line is the data smoothed over 10 adjacent wavelengths. The electrolyte is 0.1 M $TBAPF_6$ in propylene carbonate.

and 3B). The relatively small bleach corresponds in magnitude roughly to the bleach expected for charging a single NC monolayer (see Section S7 of the SI). Thicker films do not show a larger absorbance bleach, and films below a monolayer decrease in absorbance proportionally to the monolayer fraction. Given the bulky nature of the lecithin ligands, we hypothesized that electrochemical charging is limited by inefficient charge transport across the film, therefore limiting electronic doping to the NCs in direct contact with the ITO substrate, i.e., within the first NC monolayer.

We determined the electronic doping density in $CsPbBr_3$-lecithin NCs from ΔA according to $n = g\frac{\Delta A}{A_0}$, where n is the number of charges per NC; g is the state degeneracy (equal to 2 for both the $1S_e$ and $1S_h$ states in $CsPbBr_3$) and A_0 is the 1S absorbance at OCP for a single monolayer. Figure 3C shows the electronic doping density as a function of the applied potential. We observe a maximum electronic doping density of 0.25 holes/NC and 0.15 electrons/NC, corresponding to 4.8×10^{17} cm^{-3} holes and 2.9×10^{17} cm^{-3} electrons (considering the NC volume for spherical particles of 10 nm in diameter). Since the $CsPbBr_3$ unit cell has a lattice constant of 5.95 Å, this corresponds to about one charge carrier per 10^4 formula units and could be considered the onset of heavy doping. It is interesting to notice in Figure 3C the higher slope for hole injection compared to electron injection. The different slopes reflect the much more facile hole doping in comparison to electron doping. This could be due to the anodic bleach increasing and the cathodic bleach decreasing with time (Figure 4). The time-dependent bleach could underestimate electron doping relative to hole doping.

We next turn our attention to the time dependence of electrochemical doping. The hole doping level doubles by increasing the time kept at an anodic potential from 10 to 60 s (Figure 4A, C, and E). The increase in p-doping with time can be explained by sluggish hole injection from the substrate to the NC or slow ion transport across the film due to the long ligands. It can also be explained by the presence of an electrochemical side reaction; the reactant of such a side reaction is slowly consumed, leading to a slow decrease in reaction rate and an increase in hole concentration in the NC. Regardless of the mechanism, Figure 4A, C, and E shows that p-doping could be increased beyond that shown in Figure 3C by simply keeping the applied potential for longer. On the other hand, the electron doping level decreases over the time kept at a cathodic potential (Figure 4B, D, F). The decrease in n-doping with time agrees with a shift in the $1S_e$ level to more negative potentials due to the filling of trap states. Similar changes in 1Se levels due to trap filling are observed in a variety of NCs, including InAs,[28] CdSe,[71−73] and CdTe.[40] The transient traces in Figure 4 also indicate a time-dependent NC degradation; while the recovery is total for the first 35 s, after 250 (65) seconds, the anodic (cathodic) bleach recovers 90%. This shows that stability is also a matter of time scales.

https://doi.org/10.1021/jacs.6c19292
J. Am. Chem. Soc. 2026, 148, 49828−49838

The Energy Levels and Reduction Potentials Determine the Success of Doping

We analyzed the absolute positions of the $1S_e$ and $1S_h$ levels and the standard potentials of the cathodic and anodic decomposition reactions to rationalize the success of our electrochemical doping approach for $CsPbBr_3$ NCs. We estimated the position of the $1S_e$ and $1S_h$ levels of $CsPbBr_3$-lecithin NCs from the bleach onset potential (Figures 2 and 3). The $1S_e$ onset is at −1.0 V and the $1S_h$ onset is at +1.3 V, corresponding to −3.8 eV and −6.1 eV vs vacuum, respectively. The energy difference between the $1S_e$ and the $1S_h$ levels gives an electronic bandgap of 2.3 eV, in agreement with their optical bandgap of 2.4 eV. The Fermi level at OCP for the $CsPbBr_3$-lecithin NCs is at +0.5 V (−5.3 eV vs vacuum), indicating that these NCs are slightly p-doped in $TBAPF_6$/PC electrolyte. We note that the Fermi level of the dry film in air might be different.

Figure 5 compares the energy levels of the $CsPbBr_3$-lecithin NCs with literature values of bulk ligand-free $CsPbBr_3$, and

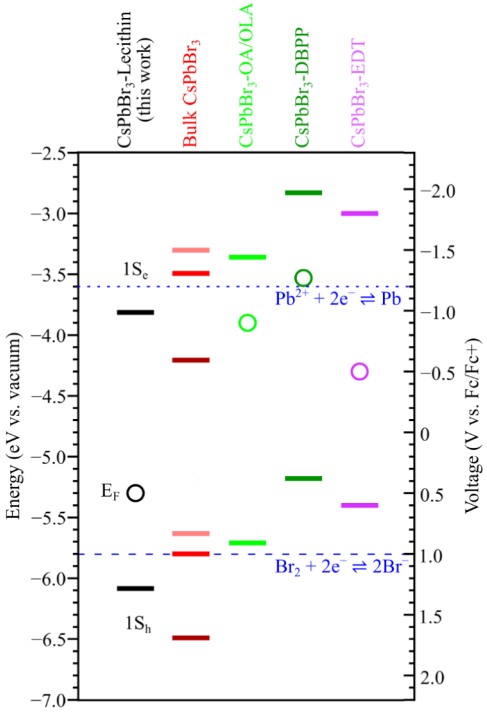

Figure 5. Energy level alignment of $CsPbBr_3$. The horizontal solid lines are the $1S_e$ and $1S_h$ energy levels (or conduction and valence bands for bulk $CsPbBr_3$) and the circles are the energy positions of the Fermi level for (from left to right): $CsPbBr_3$-lecithin NCs from this work (black), and literature values for ligand-free bulk $CsPbBr_3$ (red),[76−78] $CsPbBr_3$−OA/OLA NCs (light green),[79] $CsPbBr_3$-DBPP NCs (dark green)[79] and $CsPbBr_3$-EDT NCs (magenta).[43] The dashed lines are the standard potentials for the Pb^{2+}/Pb and Br_2/Br^- redox couples in propylene carbonate.[50]

$CsPbBr_3$ NCs capped with a mixture of oleylamine and oleic acid ($CsPbBr_3$−OA/OLA), 1,4-bis(diphenylphosphino)butane ($CsPbBr_3$-DBPP), and 1,2-ethanedithiol ($CsPbBr_3$-EDT). The most obvious difference is the lower $1S_e$ and $1S_h$ levels for $CsPbBr_3$-lecithin NCs compared to the other $CsPbBr_3$ NCs. We note that the values shown in Figure 5 compare a variety of ligand coverages, surface terminations, and measurement conditions. The absolute energy levels of NCs depend on surface termination,[74] ligand type,[52] coverage,[48] media surrounding them,[27] and measurement conditions.[75] Thus, we avoid making any conclusions on the physical origins of the lower energy levels of the $CsPbBr_3$-lecithin NCs of our work. What is important to note is that the $1S_e$ level moves below the Pb^{2+}/Pb standard potential (Figure 5, short dashed line),[50] explaining its improved stability against Pb^{2+} reduction.

Yet we observe stable electron injection to voltages much lower (−2.5 V) than the potential of Pb formation (−1.2 V). This is explained by a decrease in the $CsPbBr_3$/Pb reduction potential caused by the strong binding of lecithin ligands. The strong binding of lecithin to the NC surface decreases the solubility product of $CsPbBr_3$, and this shifts the $CsPbBr_3$/Pb reduction potential according to the Nernst equation.[43,50,80] Hence, we conclude that both the shift in $1S_e$ level to lower energy and the shift in the Pb formation reaction to higher energy contribute to the enhanced stability of $CsPbBr_3$-lecithin NCs.

On the other hand, the $1S_h$ level of the $CsPbBr_3$-lecithin NCs is lower in energy than that of the other NCs, implying that hole injection should be more difficult to accomplish for $CsPbBr_3$-lecithin NCs compared to other NCs. Br_2 formation in PC occurs above +1.0 V (Figure 5, long dashed line),[50] which is 0.3 V less positive than the $1S_h$ level of $CsPbBr_3$-lecithin NCs and therefore would not allow stable hole injection. Yet we find stable hole injection into the $CsPbBr_3$-lecithin NCs. Therefore, stable hole injection must be due to the additional stabilization provided by the ligand. In fact, we find that $CsPbBr_3$-lecithin NCs start to decompose anodically above +1.7 V, which is +0.7 V higher than Br_2 formation.

Mulder et al. previously showed that DCM offers a lower stability of $CsPbBr_3$ NCs because of the higher solubility of the apolar ligands in this solvent.[50] To showcase the improved stability that lecithin ligands offer to $CsPbBr_3$ NCs, we additionally performed electrochemical doping in DCM. Section S8 of the SI shows that electrochemical doping of $CsPbBr_3$-lecithin NCs in DCM is less stable than in PC, in agreement with the higher solubility of lecithin in DCM compared to PC. We find that spectral changes at potentials above +1.0 V in DCM are not fully reversible (unlike at even +1.7 V in PC). Nevertheless, we still find that we can inject both electrons and holes into $CsPbBr_3$-lecithin NCs even in DCM, demonstrating the improved stability provided by lecithin ligands.

Together with phosphocholines, phosphoethanolamines are among the strongest known binding ligands for $CsPbBr_3$ NCs. We find that $CsPbBr_3$ NCs passivated with 2-ammonioethyl 2-octyl-1-dodecyl phosphate ($CsPbBr_3$−PEA), a type of phosphoethanolamine ligand, in propylene carbonate exhibit improved electrochemical stability with no signs of decomposition at biases between −2.0 V and +2.5 V (Figure S28). However, we find only limited hole injection (0.02 holes/NC) and no indications of electron injection. At the moment, we do not know the reason for the lower electrochemical doping that $CsPbBr_3$−PEA shows compared to $CsPbBr_3$-lecithin. A possible reason is the bulky nature of these ligands, which makes the rate of electron transfer extremely sluggish. However, the bulky lecithin ligand did not prevent $CsPbBr_3$-lecithin NCs from showing some extent of doping. Electrochemical doping also requires ion transport across the film, and the bulky and hydrophobic nature of these ligands could impede ion transport. Lecithin has a higher degree of branching and contains ester groups that make it slightly less

https://doi.org/10.1021/jacs.6c19292
J. Am. Chem. Soc. 2026, 148, 49828−49838

hydrophobic than PEA and more likely to form an ion transport pathway across the film.

CONCLUSIONS

In summary, we demonstrate ambipolar (n- and p-) electrochemical doping of a $CsPbBr_3$ NC monolayer across a 4.2 eV window, substantially wider than the 2.4 eV bandgap. Our work outlines the design rules to make this possible. We show that electrochemical doping of $CsPbBr_3$ NCs requires protecting ligands that bind strongly to the NC. The strong binding decreases the solubility product of $CsPbBr_3$, and this shifts the reduction potential of the $CsPbBr_3$/Pb and $CsPbBr_3$/Br_2 redox couples outside the bandgap. Specifically, we show that the strong binding of lecithin, a zwitterionic ligand with a phosphocholine headgroup, protects the $CsPbBr_3$ NCs against both reductive and oxidative degradation.

This finding shows that the stability of perovskite nanocrystals is not an intrinsic property but can be enhanced by choosing the passivating ligands. Our work also establishes spectroelectrochemistry as an ideal tool to investigate the stability of perovskites. Thus, future work could use spectroelectrochemistry as a characterization tool for determining the stability of perovskites modified with different ligands.

An important finding is that electrochemical doping is confined to the NCs in close proximity with the working electrode due to the bulky nature of the lecithin ligands. This means that our work directly impacts the many scientific fields and technologies that do use monolayers and submonolayer NC films. These include the entire field of single-particle spectroscopy,[81−85] quantum optics,[86,87] nanophotonics,[88] or photocatalysis.[89−91] Technologies that sometimes use monolayer/submonolayer NC films include light-emitting diodes (LEDs),[5,13,15,24,48] micro-LEDs,[92−94] light-emitting transistors,[19,95,96] or single-photon sources.[4,83,97−99]

In addition, our work identifies the main bottleneck of electrochemical doping of perovskite nanocrystals: electronic doping is restricted to monolayer and submonolayer NC films because of the bulky ligands. This establishes future research directions for scientific fields and technologies that do require multiple layers, including X-ray detection,[100−102] solar cells,[78,103] or solar concentrators.[104−106] For these technologies to benefit from electrochemical doping, future work should use similar zwitterionic ligands with shorter tails.

We acknowledge that the prospects of integrating electrochemical doping of perovskite nanocrystals into future technologies will require further research. Specifically, it will require overcoming the key challenge of making electrochemical doping stable. We demonstrated nanocrystal stability over a few minutes at high doping levels. Yet, for integration into technologies, the NC should be stable for years. In addition, the electronic doping should also be stable upon switching off the potential, but this is often limited by the presence of impurities. Nevertheless, permanent electrochemical doping has been demonstrated for other NCs, and there are no theoretical limitations for implementing the same strategy in perovskite nanocrystals.[32,33] We hope that our work will incentivize these and other lines of research to bring electronically doped perovskite nanocrystals toward implementation in diverse technologies.

ASSOCIATED CONTENT

Data Availability Statement

The raw and processed data can be found at DOI: 10.5281/zenodo.19681245.

Supporting Information

The Supporting Information is available free of charge at https://pubs.acs.org/doi/10.1021/jacs.6c19292.

Materials and methods. $CsPbBr_3$ NC film stability in electrolyte at OCP. Spectroelectrochemical data of $CsPbBr_3$-lecithin NCs. $CsPbBr_3$ films of different thicknesses. Spectroelectrochemical data of $CsPbBr_3$-lecithin in dichloromethane. Spectroelectrochemical data of $CsPbBr_3$−PEA (PDF)

AUTHOR INFORMATION

Corresponding Authors

Yan B. Vogel − *Department of Chemical Engineering, Delft University of Technology, Delft 2629 HZ, The Netherlands; Institute of Inorganic Chemistry, Department of Chemistry and Applied Biosciences, ETH Zürich, Zürich 8093, Switzerland; Empa- Swiss Federal Laboratories for Materials Science and Technology, Dübendorf 8600, Switzerland;* orcid.org/0000-0003-1975-7292; Email: y.b.vogel@tudelft.nl

Maksym V. Kovalenko − *Institute of Inorganic Chemistry, Department of Chemistry and Applied Biosciences, ETH Zürich, Zürich 8093, Switzerland; Empa- Swiss Federal Laboratories for Materials Science and Technology, Dübendorf 8600, Switzerland;* orcid.org/0000-0002-6396-8938; Email: mvkovalenko@ethz.ch

Authors

Yesim Sahin − *Institute of Inorganic Chemistry, Department of Chemistry and Applied Biosciences, ETH Zürich, Zürich 8093, Switzerland; Empa- Swiss Federal Laboratories for Materials Science and Technology, Dübendorf 8600, Switzerland;* orcid.org/0000-0001-9717-9729

Oleksandra Ortikova − *Institute of Inorganic Chemistry, Department of Chemistry and Applied Biosciences, ETH Zürich, Zürich 8093, Switzerland; Empa- Swiss Federal Laboratories for Materials Science and Technology, Dübendorf 8600, Switzerland*

Simon C. Boehme − *Institute of Inorganic Chemistry, Department of Chemistry and Applied Biosciences, ETH Zürich, Zürich 8093, Switzerland; Empa- Swiss Federal Laboratories for Materials Science and Technology, Dübendorf 8600, Switzerland;* orcid.org/0000-0002-8399-5773

Arjan J. Houtepen − *Department of Chemical Engineering, Delft University of Technology, Delft 2629 HZ, The Netherlands;* orcid.org/0000-0001-8328-443X

Dmitry N. Dirin − *Institute of Inorganic Chemistry, Department of Chemistry and Applied Biosciences, ETH Zürich, Zürich 8093, Switzerland; Empa- Swiss Federal Laboratories for Materials Science and Technology, Dübendorf 8600, Switzerland;* orcid.org/0000-0002-5187-4555

Complete contact information is available at: https://pubs.acs.org/10.1021/jacs.6c19292

Notes

The authors declare no competing financial interest.

■ ACKNOWLEDGMENTS

Y.B.V. acknowledges the support from the Swiss National Science Foundation (P5R5PN_222309). This publication was created as part of NCCR Catalysis (grant number 225147), a National Centre of Competence in Research funded by the Swiss National Science Foundation. Y.B.V. thanks Xiaohui Liu and Hua Chen for their help with the XPS measurements.

■ REFERENCES

(1) Puthenpurayil, J.; Cheng, O. H.-C.; Qiao, T.; Rossi, D.; Son, D. H. On the Determination of Absorption Cross Section of Colloidal Lead Halide Perovskite Quantum Dots. *J. Chem. Phys.* **2019**, *151*, 154706.

(2) Maes, J.; Balcaen, L.; Drijvers, E.; Zhao, Q.; De Roo, J.; Vantomme, A.; Vanhaecke, F.; Geiregat, P.; Hens, Z. Light Absorption Coefficient of Cspbbr3 Perovskite Nanocrystals. *J. Phys. Chem. Lett.* **2018**, *9*, 3093−3097.

(3) Swarnkar, A.; Chulliyil, R.; Ravi, V. K.; Irfanullah, M.; Chowdhury, A.; Nag, A. Colloidal Cspbbr3 Perovskite Nanocrystals: Luminescence Beyond Traditional Quantum Dots. *Angew. Chem., Int. Ed.* **2015**, *127*, 15644−15648.

(4) Rainò, G.; Yazdani, N.; Boehme, S. C.; Kober-Czerny, M.; Zhu, C.; Krieg, F.; Rossell, M. D.; Erni, R.; Wood, V.; Infante, I.; et al. Ultra-Narrow Room-Temperature Emission from Single Cspbbr3 Perovskite Quantum Dots. *Nat. Commun.* **2022**, *13*, 2587.

(5) Shi, W.; Zhang, X.; Xie, C.; Chen, H. S.; Yang, P. Blue Emitting Cspbbr3: High Quantum Confinement Effect and Well-Adjusted Shapes (Nanorods, Nanoplates, and Cubes). toward White Light Emitting Diodes. *Adv. Opt. Mater.* **2024**, *12*, 2302129.

(6) Dutta, A.; Behera, R. K.; Pal, P.; Baitalik, S.; Pradhan, N. Near-Unity Photoluminescence Quantum Efficiency for All Cspbx3 (X = Cl, Br, and I). Perovskite Nanocrystals: A Generic Synthesis Approach. *Angew. Chem., Int. Ed.* **2019**, *58*, 5552−5556.

(7) Di Stasio, F.; Christodoulou, S.; Huo, N.; Konstantatos, G. Near-Unity Photoluminescence Quantum Yield in Cspbbr3 Nanocrystal Solid-State Films Via Postsynthesis Treatment with Lead Bromide. *Chem. Mater.* **2017**, *29*, 7663−7667.

(8) Dutt, V. G. V.; Akhil, S.; Singh, R.; Palabathuni, M.; Mishra, N. Year-Long Stability and near-Unity Photoluminescence Quantum Yield of Cspbbr3 Perovskite Nanocrystals by Benzoic Acid Post-Treatment. *J. Phys. Chem. C* **2022**, *126*, 9502−9508.

(9) Zhong, Q.; Cao, M.; Xu, Y.; Li, P.; Zhang, Y.; Hu, H.; Yang, D.; Xu, Y.; Wang, L.; Li, Y.; et al. L-Type Ligand-Assisted Acid-Free Synthesis of Cspbbr3 Nanocrystals with near-Unity Photoluminescence Quantum Yield and High Stability. *Nano Lett.* **2019**, *19*, 4151−4157.

(10) Kovalenko, M. V.; Protesescu, L.; Bodnarchuk, M. I. Properties and Potential Optoelectronic Applications of Lead Halide Perovskite Nanocrystals. *Science* **2017**, *358*, 745−750.

(11) Protesescu, L.; Yakunin, S.; Bodnarchuk, M. I.; Krieg, F.; Caputo, R.; Hendon, C. H.; Yang, R. X.; Walsh, A.; Kovalenko, M. V. Nanocrystals of Cesium Lead Halide Perovskites (Cspbx3, X = Cl, Br, and I): Novel Optoelectronic Materials Showing Bright Emission with Wide Color Gamut. *Nano Lett.* **2015**, *15*, 3692−3696.

(12) Kirmani, A. R.; Woodhouse, M.; Luther, J. M. Technoeconomic Model Suggests Scaling-up Perovskite Quantum Dots for Optoelectronics Warrants Improved Synthesis Yield, Solvent Recycling, and Automation. *ACS Energy Lett.* **2022**, *7*, 1255−1259.

(13) Alberola-Borràs, J.-A.; da Silva, T. C. A.; Franco, I. P.; Sánchez, R. S.; Julián-López, B.; Mora-Seró, I.; Vidal, R. Environmental Impacts and Cost Analysis of Perovskite Nanocrystals for Light-Emitting Diode Applications. *Adv. Sustainable Syst.* **2025**, *9*, No. e00516.

(14) Dong, Y.; Zhao, Y.; Zhang, S.; Dai, Y.; Liu, L.; Li, Y.; Chen, Q. Recent Advances toward Practical Use of Halide Perovskite Nanocrystals. *J. Mater. Chem. A* **2018**, *6*, 21729−21746.

(15) Li, X.; Wu, Y.; Zhang, S.; Cai, B.; Gu, Y.; Song, J.; Zeng, H. Cspbx3 Quantum Dots for Lighting and Displays: Room-Temperature Synthesis, Photoluminescence Superiorities, Underlying Origins and White Light-Emitting Diodes. *Adv. Funct. Mater.* **2016**, *26*, 2435−2445.

(16) Euvrard, J.; Yan, Y.; Mitzi, D. B. Electrical Doping in Halide Perovskites. *Nat. Rev. Mater.* **2021**, *6*, 531−549.

(17) Amerling, E.; Lu, H.; Larson, B. W.; Maughan, A. E.; Phillips, A.; Lafalce, E.; Whittaker-Brooks, L.; Berry, J. J.; Beard, M. C.; Vardeny, Z. V.; et al. A Multi-Dimensional Perspective on Electronic Doping in Metal Halide Perovskites. *ACS Energy Lett.* **2021**, *6*, 1104−1123.

(18) Zhou, S.; Ma, Y.; Zhou, G.; Xu, X.; Qin, M.; Li, Y.; Hsu, Y.-J.; Hu, H.; Li, G.; Zhao, N.; et al. Ag-Doped Halide Perovskite Nanocrystals for Tunable Band Structure and Efficient Charge Transport. *ACS Energy Lett.* **2019**, *4*, 534−541.

(19) Zhou, S.; Zhou, G.; Li, Y.; Xu, X.; Hsu, Y.-J.; Xu, J.; Zhao, N.; Lu, X. Understanding Charge Transport in All-Inorganic Halide Perovskite Nanocrystal Thin-Film Field Effect Transistors. *ACS Energy Lett.* **2020**, *5*, 2614−2623.

(20) Begum, R.; Parida, M. R.; Abdelhady, A. L.; Murali, B.; Alyami, N. M.; Ahmed, G. H.; Hedhili, M. N.; Bakr, O. M.; Mohammed, O. F. Engineering Interfacial Charge Transfer in Cspbbr3 Perovskite Nanocrystals by Heterovalent Doping. *J. Am. Chem. Soc.* **2017**, *139*, 731−737.

(21) Sabino, F. P.; Zunger, A.; Dalpian, G. M. Intrinsic Doping Limitations in Inorganic Lead Halide Perovskites. *Mater. Horiz.* **2022**, *9*, 791−803.

(22) Rosales, B. A.; Schutt, K.; Berry, J. J.; Wheeler, L. M. Leveraging Low-Energy Structural Thermodynamics in Halide Perovskites. *ACS Energy Lett.* **2023**, *8*, 1705−1715.

(23) Gaulding, E. A.; Hao, J.; Kang, H. S.; Miller, E. M.; Habisreutinger, S. N.; Zhao, Q.; Hazarika, A.; Sercel, P. C.; Luther, J. M.; Blackburn, J. L. Conductivity Tuning Via Doping with Electron Donating and Withdrawing Molecules in Perovskite Cspbi3 Nanocrystal Films. *Adv. Mater.* **2019**, *31*, 1902250.

(24) Xia, Z.; Jiang, J.; Wang, A.; An, D.; Li, Z.; Zheng, H.; Yin, Z.; He, G.; You, J.; Zhang, X. Overall Performance Improvement of Perovskite Green Leds by Cspbbr3&Cs4pbbr6 Nanocrystals and Molecular Doping. *Adv. Mater.* **2025**, *37*, 2506187.

(25) Huang, G.; Wang, C.; Xu, S.; Zong, S.; Lu, J.; Wang, Z.; Lu, C.; Cui, Y. Postsynthetic Doping of Mncl2Molecules into Preformed Cspbbr3 Perovskite Nanocrystals Via a Halide Exchange-Driven Cation Exchange. *Adv. Mater.* **2017**, *29*, 1700095.

(26) Gélvez-Rueda, M. C.; Fridriksson, M. B.; Dubey, R. K.; Jager, W. F.; van der Stam, W.; Grozema, F. C. Overcoming the Exciton Binding Energy in Two-Dimensional Perovskite Nanoplatelets by Attachment of Conjugated Organic Chromophores. *Nat. Commun.* **2020**, *11*, 1901.

(27) Vogel, Y. B.; Pham, L. N.; Stam, M.; Ubbink, R. F.; Coote, M. L.; Houtepen, A. J. Solvation Shifts the Band-Edge Position of Colloidal Quantum Dots by Nearly 1 Ev. *J. Am. Chem. Soc.* **2024**, *146*, 9928−9938.

(28) Vogel, Y. B.; Tao, R.; Chen, H.; Ferraresi, L. J. A.; Boehme, S. C.; Dirin, D. N.; Shorubalko, I.; Houtepen, A. J.; Kovalenko, M. V. Electrochemical Control over Electron Density of Inas Quantum Dots. *J. Am. Chem. Soc.* **2026**, *148*, 3938−3943.

(29) Yu, D.; Wang, C.; Guyot-Sionnest, P. N-Type Conducting Cdse Nanocrystal Solids. *Science* **2003**, *300*, 1277−1280.

(30) Shim, M.; Guyot-Sionnest, P. N-Type Colloidal Semiconductor Nanocrystals. *Nature* **2000**, *407*, 981−983.

(31) Ubbink, R. F.; Gudjonsdottir, S.; Vogel, Y. B.; Houtepen, A. J. Numerical Model to Simulate Electrochemical Charging of Nanocrystal Films. *J. Phys. Chem. C* **2023**, *127*, 9896−9902.

https://doi.org/10.1021/jacs.6c19292
J. Am. Chem. Soc. 2026, 148, 49828−49838

(32) Gudjonsdottir, S.; Houtepen, A. J. Permanent Electrochemical Doping of Quantum Dots and Semiconductor Polymers. *Adv. Funct. Mater.* **2020**, *30*, 2004789.
(33) Eren, H.; Bednarz, R. J.-R.; Alimoradi Jazi, M.; Donk, L.; Gudjonsdottir, S.; Bohländer, P.; Eelkema, R.; Houtepen, A. J. Permanent Electrochemical Doping of Quantum Dot Films through Photopolymerization of Electrolyte Ions. *Chem. Mater.* **2022**, *34*, 4019−4028.
(34) Hoyer, P.; Weller, H. Potential-Dependent Electron Injection in Nanoporous Colloidal Zno Films. *J. Phys. Chem.* **1995**, *99*, 14096−14100.
(35) Vogel, Y. B.; Stam, M.; Mulder, J. T.; Houtepen, A. J. Long-Range Charge Transport Via Redox Ligands in Quantum Dot Assemblies. *ACS Nano* **2022**, *16*, 21216−21224.
(36) Ding, Z.; Quinn, B. M.; Haram, S. K.; Pell, L. E.; Korgel, B. A.; Bard, A. J. Electrochemistry and Electrogenerated Chemiluminescence from Silicon Nanocrystal Quantum Dots. *Science* **2002**, *296*, 1293−1297.
(37) Wehrenberg, B. L.; Guyot-Sionnest, P. Electron and Hole Injection in Pbse Quantum Dot Films. *J. Am. Chem. Soc.* **2003**, *125*, 7806−7807.
(38) Ubbink, R. F.; Vogel, Y. B.; Stam, M.; Chen, H.; Houtepen, A. J. Where Do the Electrons Go? Studying Loss Processes in the Electrochemical Charging of Semiconductor Nanomaterials. *Chem. Mater.* **2025**, *37*, 736−745.
(39) Boehme, S. C.; Walvis, T. A.; Infante, I.; Grozema, F. C.; Vanmaekelbergh, D.; Siebbeles, L. D. A.; Houtepen, A. J. Electrochemical Control over Photoinduced Electron Transfer and Trapping in Cdse-Cdte Quantum-Dot Solids. *ACS Nano* **2014**, *8*, 7067−7077.
(40) van der Stam, W.; du Fossé, I.; Grimaldi, G.; Monchen, J. O. V.; Kirkwood, N.; Houtepen, A. J. Spectroelectrochemical Signatures of Surface Trap Passivation on Cdte Nanocrystals. *Chem. Mater.* **2018**, *30*, 8052−8061.
(41) Liu, H.; Keuleyan, S.; Guyot-Sionnest, P. N- and P-Type Hgte Quantum Dot Films. *J. Phys. Chem. C* **2012**, *116*, 1344−1349.
(42) Chen, M.; Guyot-Sionnest, P. Reversible Electrochemistry of Mercury Chalcogenide Colloidal Quantum Dot Films. *ACS Nano* **2017**, *11*, 4165−4173.
(43) Mulder, J. T.; du Fossé, I.; Alimoradi Jazi, M.; Manna, L.; Houtepen, A. J. Electrochemical P-Doping of Cspbbr3 Perovskite Nanocrystals. *ACS Energy Lett.* **2021**, *6*, 2519−2525.
(44) Saha, S. K.; Guyot-Sionnest, P. Mid-Infrared Intraband Transitions in Inas Colloidal Quantum Dots. *ACS Nano* **2026**, *20*, 5199−5207.
(45) Samu, G. F.; Scheidt, R. A.; Kamat, P. V.; Janáky, C. Electrochemistry and Spectroelectrochemistry of Lead Halide Perovskite Films: Materials Science Aspects and Boundary Conditions. *Chem. Mater.* **2018**, *30*, 561−569.
(46) Stam, M.; Chen, H.; Vogel, Y. B.; Stavast, I.; van Leeuwen, M.; Ubbink, R. F.; van Silfhout, N.; van der Made, C. F. A.; Giordano, L.; Schiettecatte, P.; et al. Electrochemical Stability and Trap-State-Mediated Photoluminescence Modulation of Inp-Based Quantum Dots. *Chem. Mater.* **2026**, *38*, 1407−1414.
(47) Hettiger, T.; Jayabalan, R.; Sarkar, A.; Hiller, J. L.; Nusshör, M.; Andrienko, D.; Brütting, W.; Scheele, M. Impact of Ligand-Mediated Inductive Effects on Electrochemical P-Doping of Cspbbr3 Nanocrystals. *ACS Energy Lett.* **2026**, *11*, 567−572.
(48) Jayabalan, R.; Hanumantharaju, G. K.; Hettiger, T.; Sarkar, A.; Zu, F.; Ullrich, A.; Abfalterer, A.; Urban, A. S.; Koch, N.; Andrienko, D.; et al. Optimizing Carrier Balance in Cspbbr3 Nanocrystal Leds: The Role of Alkyl Ligands and Polar Electron Transport Layers. *Adv. Opt. Mater.* **2025**, *13*, No. e01361.
(49) Hettiger, T.; Hiller, J. L.; Hodak, R.; Eberle, M.; Meixner, A. J.; Scheele, M. Spatial Mapping of Electrochemical Hole-Injection into Supercrystals of Perovskite Nanocrystals. *ChemRxiv* 2026. .
(50) Mulder, J. T.; Monchen, J. O. V.; Vogel, Y. B.; Lin, C. T.; Drago, F.; Caselli, V. M.; Saikumar, N.; Savenije, T. J.; Houtepen, A. J. Orthogonal Electrochemical Stability of Bulk and Surface in Lead Halide Perovskite Thin Films and Nanocrystals. *J. Am. Chem. Soc.* **2024**, *146*, 24415−24425.
(51) Heo, S.; Roh, K.; Zhang, F.; Tignor, S. E.; Bocarsly, A. B.; Kahn, A.; Rand, B. P. Electrochemically N-Doped Cspbbr3 Nanocrystal Thin Films. *ACS Energy Lett.* **2022**, *7*, 211−216.
(52) Brown, P. R.; Kim, D.; Lunt, R. R.; Zhao, N.; Bawendi, M. G.; Grossman, J. C.; Bulović, V. Energy Level Modification in Lead Sulfide Quantum Dot Thin Films through Ligand Exchange. *ACS Nano* **2014**, *8*, 5863−5872.
(53) Kroupa, D. M.; Vörös, M.; Brawand, N. P.; McNichols, B. W.; Miller, E. M.; Gu, J.; Nozik, A. J.; Sellinger, A.; Galli, G.; Beard, M. C. Tuning Colloidal Quantum Dot Band Edge Positions through Solution-Phase Surface Chemistry Modification. *Nat. Commun.* **2017**, *8*, 15257.
(54) Gudjonsdottir, S.; van der Stam, W.; Kirkwood, N.; Evers, W. H.; Houtepen, A. J. The Role of Dopant Ions on Charge Injection and Transport in Electrochemically Doped Quantum Dot Films. *J. Am. Chem. Soc.* **2018**, *140*, 6582−6590.
(55) Mastrippolito, D.; Ibrahim, M.; Yeromina, O.; Cavallo, M.; Strobbia, G.; Bossavit, E.; Roh, J.; Paye, M.; Khalili, A.; Prado, Y.; et al. Adjusting the Energy Levels of Hgte and Inas Nanocrystals with Alkali Ions. *J. Phys. Chem. C* **2026**, *130*, 449−456.
(56) Degbevi, M.; Balliew, W. L.; Handunge, K. U.; Oliver, A. G.; Tsui, E. Y. Ligand Basicity Modulates Metal Cation Reduction Potentials at Colloidal Cadmium Chalcogenide Quantum Dot Surfaces. *J. Am. Chem. Soc.* **2025**, *147*, 18257−18266.
(57) Ciampi, S.; Harper, J. B.; Gooding, J. J. Wet Chemical Routes to the Assembly of Organic Monolayers on Silicon Surfaces Via the Formation of Si−C Bonds: Surface Preparation, Passivation and Functionalization. *Chem. Soc. Rev.* **2010**, *39*, 2158−2183.
(58) Ciampi, S.; Böcking, T.; Kilian, K. A.; James, M.; Harper, J. B.; Gooding, J. J. Functionalization of Acetylene-Terminated Monolayers on Si(100). Surfaces: a Click Chemistry Approach. *Langmuir* **2007**, *23*, 9320−9329.
(59) Vogel, Y. B.; Gooding, J. J.; Ciampi, S. Light-Addressable Electrochemistry at Semiconductor Electrodes: Redox Imaging, Mask-Free Lithography and Spatially Resolved Chemical and Biological Sensing. *Chem. Soc. Rev.* **2019**, *48*, 3723−3739.
(60) Vogel, Y. B.; Molina, A.; Gonzalez, J.; Ciampi, S. Quantitative Analysis of Cyclic Voltammetry of Redox Monolayers Adsorbed on Semiconductors: Isolating Electrode Kinetics, Lateral Interactions, and Diode Currents. *Anal. Chem.* **2019**, *91*, 5929−5937.
(61) Ciampi, S.; Eggers, P. K.; Le Saux, G.; James, M.; Harper, J. B.; Gooding, J. J. Silicon (100). Electrodes Resistant to Oxidation in Aqueous Solutions: An Unexpected Benefit of Surface Acetylene Moieties. *Langmuir* **2009**, *25*, 2530−2539.
(62) Krieg, F.; Ochsenbein, S. T.; Yakunin, S.; ten Brinck, S.; Aellen, P.; Süess, A.; Clerc, B.; Guggisberg, D.; Nazarenko, O.; Shynkarenko, Y.; et al. Colloidal Cspbx3 (X = Cl, Br, I) Nanocrystals 2.0: Zwitterionic Capping Ligands for Improved Durability and Stability. *ACS Energy Lett.* **2018**, *3*, 641−646.
(63) Morad, V.; Stelmakh, A.; Svyrydenko, M.; Feld, L. G.; Boehme, S. C.; Aebli, M.; Affolter, J.; Kaul, C. J.; Schrenker, N. J.; Bals, S.; et al. Designer Phospholipid Capping Ligands for Soft Metal Halide Nanocrystals. *Nature* **2024**, *626*, 542−548.
(64) Berezovska, Y.; Sabisch, S.; Bernasconi, C.; Sahin, Y.; Bertolotti, F.; Guagliardi, A.; Bodnarchuk, M. I.; Dirin, D. N.; Kovalenko, M. V. Tightly yet Dynamically Bound Aliphatic Guanidinium Ligands for Lead Halide Perovskite Nanocrystals. *J. Am. Chem. Soc.* **2025**, *147*, 35446−35455.
(65) Akkerman, Q. A.; Nguyen, T. P. T.; Boehme, S. C.; Montanarella, F.; Dirin, D. N.; Wechsler, P.; Beiglböck, F.; Rainò, G.; Erni, R.; Katan, C.; et al. Controlling the Nucleation and Growth Kinetics of Lead Halide Perovskite Quantum Dots. *Science* **2022**, *377*, 1406−1412.
(66) Krieg, F.; Ong, Q. K.; Burian, M.; Rainò, G.; Naumenko, D.; Amenitsch, H.; Süess, A.; Grotevent, M. J.; Krumeich, F.; Bodnarchuk, M. I.; et al. Stable Ultraconcentrated and Ultradilute

Colloids of Cspbx3 (X = Cl, Br) Nanocrystals Using Natural Lecithin as a Capping Ligand. *J. Am. Chem. Soc.* **2019**, *141*, 19839−19849.
(67) Sarkar, D.; Stelmakh, A.; Karmakar, A.; Aebli, M.; Krieg, F.; Bhattacharya, A.; Pawsey, S.; Kovalenko, M. V.; Michaelis, V. K. Surface Structure of Lecithin-Capped Cesium Lead Halide Perovskite Nanocrystals Using Solid-State and Dynamic Nuclear Polarization Nmr Spectroscopy. *ACS Nano* **2024**, *18*, 21894−21910.
(68) Blundell, S. A.; Guet, C. All-Order Correlation of Single Excitons in Nanocrystals Using a $K\Ifmmode\Cdot\Else\Textperiodcentered\Fi{}P$ Envelope-Function Approach: Application to Lead Halide Perovskites. *Phys. Rev. B* **2022**, *105*, 155420.
(69) Zhang, L.; Vogel, Y. B.; Noble, B. B.; Gonçales, V. R.; Darwish, N.; Brun, A. L.; Gooding, J. J.; Wallace, G. G.; Coote, M. L.; Ciampi, S. Tempo Monolayers on Si(100) Electrodes: Electrostatic Effects by the Electrolyte and Semiconductor Space-Charge on the Electroactivity of a Persistent Radical. *J. Am. Chem. Soc.* **2016**, *138*, 9611−9619.
(70) Gudjonsdottir, S.; Koopman, C.; Houtepen, A. J. Enhancing the Stability of the Electron Density in Electrochemically Doped Zno Quantum Dots. *J. Chem. Phys.* **2019**, *151*, 144708.
(71) Chen, H.; Ubbink, R. F.; Olsthoorn, R. A.; Stam, M.; 't Hoen, J.; Savenije, T. J.; Houtepen, A. J. Potential of Electrochemical Charge Injection for Quantum Dot Light-Emitting Devices. *Chem. Mater.* **2025**, *37*, 4435−4444.
(72) van der Stam, W.; Grimaldi, G.; Geuchies, J. J.; Gudjonsdottir, S.; van Uffelen, P. T.; van Overeem, M.; Brynjarsson, B.; Kirkwood, N.; Houtepen, A. J. Electrochemical Modulation of the Photophysics of Surface-Localized Trap States in Core/Shell/(Shell) Quantum Dot Films. *Chem. Mater.* **2019**, *31*, 8484−8493.
(73) Boehme, S. C.; Vanmaekelbergh, D. L.; Evers, W. H.; Siebbeles, L. D. A.; Houtepen, A. J. In Situ Spectroelectrochemical Determination of Energy Levels and Energy Level Offsets in Quantum-Dot Heterojunctions. *J. Phys. Chem. C* **2016**, *120*, 5164−5173.
(74) ten Brinck, S.; Infante, I. S. T. Morphology, and Bright Photoluminescence of Cesium Lead Halide Perovskite Nanocrystals. *ACS Energy Lett.* **2016**, *1*, 1266−1272.
(75) Miller, E. M.; Kroupa, D. M.; Zhang, J.; Schulz, P.; Marshall, A. R.; Kahn, A.; Lany, S.; Luther, J. M.; Beard, M. C.; Perkins, C. L.; et al. Revisiting the Valence and Conduction Band Size Dependence of Pbs Quantum Dot Thin Films. *ACS Nano* **2016**, *10*, 3302−3311.
(76) Endres, J.; Egger, D. A.; Kulbak, M.; Kerner, R. A.; Zhao, L.; Silver, S. H.; Hodes, G.; Rand, B. P.; Cahen, D.; Kronik, L.; et al. Valence and Conduction Band Densities of States of Metal Halide Perovskites: A Combined Experimental−Theoretical Study. *J. Phys. Chem. Lett.* **2016**, *7*, 2722−2729.
(77) Tao, S.; Schmidt, I.; Brocks, G.; Jiang, J.; Tranca, I.; Meerholz, K.; Olthof, S. Absolute Energy Level Positions in Tin- and Lead-Based Halide Perovskites. *Nat. Commun.* **2019**, *10*, 2560.
(78) Liang, J.; Wang, C.; Wang, Y.; Xu, Z.; Lu, Z.; Ma, Y.; Zhu, H.; Hu, Y.; Xiao, C.; Yi, X.; et al. All-Inorganic Perovskite Solar Cells. *J. Am. Chem. Soc.* **2016**, *138*, 15829−15832.
(79) Hassan, M. S.; Basera, P.; Khan, B.; Portniagin, A. S.; Vighnesh, K.; Wu, Y.; Rusanov, D. A.; Babak, M.; He, J.-H.; Bajdich, M.; et al. Bidentate Lewis Base Ligand-Mediated Surface Stabilization and Modulation of the Electronic Structure of Cspbbr3 Perovskite Nanocrystals. *J. Am. Chem. Soc.* **2025**, *147*, 862−873.
(80) Bard, A. J.; Faulkner, L. R.; White, H. S. *Electrochemical Methods: fundamentals and Applications*; John Wiley & Sons, 2022.
(81) Feld, L. G.; Kolomiiets, O.; Shahin, N. A.; Sabisch, S.; Rajan, A.; Rainò, G.; Kovalenko, M. V. Single-Particle Fret Probes Heterogeneity in the Ligand Shell of Colloidal Perovskite Quantum Dots. *Adv. Mater.* **2026**, No. e75051.
(82) Sekh, T. V.; Kim, T.; Sabisch, S.; Bertolotti, F.; Caliò, L.; Galisteo-López, J. F.; Coto-Ruiz, F. J.; Santiago-Andrades, L.; Guagliardi, A.; Masciocchi, N.; et al. Ligand-Engineered Methylammonium Lead Bromide Nanoplatelets: Single-Photon Emission and Strong Light-Matter Coupling. *ACS Nano* **2026**, *20*, 11358−11373.
(83) Boehme, S. C.; Nguyen, T. P. T.; Zhu, C.; Cherniukh, I.; Feld, L. G.; Dirin, D. N.; Bodnarchuk, M. I.; Katan, C.; Even, J.; Kovalenko, M. V.; et al. Single-Photon Superabsorption in Cspbbr3 Perovskite Quantum Dots. *Nat. Photonics* **2025**, *19*, 864−870.
(84) Zhu, C.; Boehme, S. C.; Feld, L. G.; Moskalenko, A.; Dirin, D. N.; Mahrt, R. F.; Stöferle, T.; Bodnarchuk, M. I.; Efros, A. L.; Sercel, P. C.; et al. Single-Photon Superradiance in Individual Caesium Lead Halide Quantum Dots. *Nature* **2024**, *626*, 535−541.
(85) Zhu, C.; Marczak, M.; Feld, L.; Boehme, S. C.; Bernasconi, C.; Moskalenko, A.; Cherniukh, I.; Dirin, D.; Bodnarchuk, M. I.; Kovalenko, M. V.; et al. Room-Temperature, Highly Pure Single-Photon Sources from All-Inorganic Lead Halide Perovskite Quantum Dots. *Nano Lett.* **2022**, *22*, 3751−3760.
(86) Kaplan, A. E. K.; Krajewska, C. J.; Proppe, A. H.; Sun, W.; Sverko, T.; Berkinsky, D. B.; Utzat, H.; Bawendi, M. G. Hong−Ou−Mandel Interference in Colloidal Cspbbr3 Perovskite Nanocrystals. *Nat. Photonics* **2023**, *17*, 775−780.
(87) Shi, J.; Shen, Y.; Pan, F.; Sun, W.; Mangu, A.; Shi, C.; McKeown-Green, A.; Moradifar, P.; Bawendi, M. G.; Moerner, W. E.; et al. Solution-Phase Sample-Averaged Single-Particle Spectroscopy of Quantum Emitters with Femtosecond Resolution. *Nat. Mater.* **2024**, *23*, 1063−1069.
(88) Makarov, S.; Furasova, A.; Tiguntseva, E.; Hemmetter, A.; Berestennikov, A.; Pushkarev, A.; Zakhidov, A.; Kivshar, Y. Halide-Perovskite Resonant Nanophotonics. *Adv. Opt. Mater.* **2019**, *7*, 1800784.
(89) Sahin, Y.; Sabisch, S.; Feld, L. G.; Tao, R.; Morad, V.; Amberg, W. M.; Lindner, H.; Rainò, G.; Carreira, E. M.; Kovalenko, M. V.; et al. Surface-Governed Photoredox Reactivity of Cspbbr3 Quantum Dots. *Nano Lett.* **2026**, *26*, 3107−3116.
(90) Feld, L. G.; Sahin, Y.; Sabisch, S.; Rainò, G.; Kovalenko, M. V. Single-Catalyst Operando Photoluminescence Spectroscopy of Perovskite Quantum-Dot-Driven Photoredox Reactions. *ChemRxiv* 2026, *2026*. .
(91) Amberg, W. M.; Lindner, H.; Sahin, Y.; Staudinger, E.; Morad, V.; Sabisch, S.; Feld, L. G.; Li, Y.; Dirin, D. N.; Kovalenko, M. V.; et al. Ligand Influence on the Performance of Cesium Lead Bromide Perovskite Quantum Dots in Photocatalytic C(Sp(3))-H Bromination Reactions. *J. Am. Chem. Soc.* **2025**, *147*, 8548−8558.
(92) Lian, Y.; Wang, Y.; Yuan, Y.; Ren, Z.; Tang, W.; Liu, Z.; Xing, S.; Ji, K.; Yuan, B.; Yang, Y.; et al. Downscaling Micro- and Nano-Perovskite Leds. *Nature* **2025**, *640*, 62−68.
(93) Yuan, M.; Feng, J.; Li, H.; Gao, H.; Qiu, Y.; Jiang, L.; Wu, Y. Remote Epitaxial Crystalline Perovskites for Ultrahigh-Resolution Micro-Led Displays. *Nat. Nanotechnol.* **2025**, *20*, 381−387.
(94) Gong, T.; Shi, J.; Zhang, Y.; Bai, W.; Xuan, T.; Zhou, T.; Huang, K.; Xie, R.-J. Rare Earth-Doped Perovskite Quantum Dot Microspheres for Micro-Led Displays. *ACS Energy Lett.* **2025**, *10*, 5012−5019.
(95) Kim, D.-K.; Choi, D.; Park, M.; Jeong, K. S.; Choi, J.-H. Cesium Lead Bromide Quantum Dot Light-Emitting Field-Effect Transistors. *ACS Appl. Mater. Interfaces* **2020**, *12*, 21944−21951.
(96) Park, Y. J.; Kim, M.; Song, A.; Kim, J. Y.; Chung, K.-B.; Walker, B.; Seo, J. H.; Wang, D. H. Light-Emitting Transistors with High Color Purity Using Perovskite Quantum Dot Emitters. *ACS Appl. Mater. Interfaces* **2020**, *12*, 35175−35180.
(97) Park, Y.-S.; Guo, S.; Makarov, N. S.; Klimov, V. I. Room Temperature Single-Photon Emission from Individual Perovskite Quantum Dots. *ACS Nano* **2015**, *9*, 10386−10393.
(98) Utzat, H.; Sun, W.; Kaplan, A. E. K.; Krieg, F.; Ginterseder, M.; Spokoyny, B.; Klein, N. D.; Shulenberger, K. E.; Perkinson, C. F.; Kovalenko, M. V.; et al. Coherent Single-Photon Emission from Colloidal Lead Halide Perovskite Quantum Dots. *Science* **2019**, *363*, 1068−1072.
(99) Gorji, S.; Pashaei Adl, H.; Gualdrón-Reyes, A. F.; Sánchez Sánchez, A.; Sánchez Alarcón, R. I.; Pareja-Rivera, C.; Mora-Seró, I.; Martínez Pastor, J. P.; Muñoz Matutano, G. Enhanced Optical Stability of All Inorganic Perovskite Nanocrystals for Single Photon Emission. *Adv. Opt. Mater.* **2025**, *13*, 2403441.

(100) Morad, V.; Shynkarenko, Y.; Yakunin, S.; Brumberg, A.; Schaller, R. D.; Kovalenko, M. V. Disphenoidal Zero-Dimensional Lead, Tin, and Germanium Halides: Highly Emissive Singlet and Triplet Self-Trapped Excitons and X-Ray Scintillation. *J. Am. Chem. Soc.* **2019**, *141*, 9764−9768.
(101) Sakhatskyi, K.; Bhardwaj, A.; Matt, G. J.; Yakunin, S.; Kovalenko, M. V. A Decade of Lead Halide Perovskites for Direct-Conversion X-Ray and Gamma Detection: Technology Readiness Level and Challenges. *Adv. Mater.* **2025**, *37*, 2418465.
(102) Chen, Q.; Wu, J.; Ou, X.; Huang, B.; Almutlaq, J.; Zhumekenov, A. A.; Guan, X.; Han, S.; Liang, L.; Yi, Z.; et al. All-Inorganic Perovskite Nanocrystal Scintillators. *Nature* **2018**, *561*, 88−93.
(103) Akkerman, Q. A.; Gandini, M.; Di Stasio, F.; Rastogi, P.; Palazon, F.; Bertoni, G.; Ball, J. M.; Prato, M.; Petrozza, A.; Manna, L. Strongly Emissive Perovskite Nanocrystal Inks for High-Voltage Solar Cells. *Nat. Energy* **2017**, *2*, 16194.
(104) Meinardi, F.; Akkerman, Q. A.; Bruni, F.; Park, S.; Mauri, M.; Dang, Z.; Manna, L.; Brovelli, S. Doped Halide Perovskite Nanocrystals for Reabsorption-Free Luminescent Solar Concentrators. *ACS Energy Lett.* **2017**, *2*, 2368−2377.
(105) Zhao, H.; Sun, R.; Wang, Z.; Fu, K.; Hu, X.; Zhang, Y. Zero-Dimensional Perovskite Nanocrystals for Efficient Luminescent Solar Concentrators. *Adv. Funct. Mater.* **2019**, *29*, 1902262.
(106) Zhou, N.; Wang, D.; Bao, Y.; Zhu, R.; Yang, P.; Song, L. A Review of Perovskite Nanocrystal Applications in Luminescent Solar Concentrators. *Adv. Opt. Mater.* **2023**, *11*, 2202681.

https://doi.org/10.1021/jacs.6c19292
J. Am. Chem. Soc. 2026, 148, 49828−49838